Self-referencing, spectral interferometric probing of the onset time of relativistic transparency in intense laser-foil interactions

S.D.R. Williamson,[1] R. Wilson,[1] M. King,[1] M. Duff,[1] B. Gonzalez-Izquierdo,[1] Z.E. Davidson,[1] A. Higginson,[1] N. Booth,[2] S. Hawkes,[2] D. Neely,[2,1] R.J. Gray,[1] and P. McKenna[1,*]

[1] *SUPA Department of Physics, University of Strathclyde, Glasgow G4 0NG, United Kingdom*
[2] *Central Laser Facility, STFC Rutherford Appleton Laboratory, Oxfordshire OX11 0QX, United Kingdom*

(Dated: August 14, 2020)

Irradiation of an ultrathin foil target by a high intensity laser pulse drives collective electron motion and the generation of strong electrostatic fields, resulting in ultrabright sources of high-order harmonics and energetic ions. The ion energies can be significantly enhanced if the foil undergoes relativistic self-induced transparency during the interaction, with the degree of enhancement depending in part on the onset time of transparency. We report on a simple and effective approach to diagnose the time during the interaction at which the foil becomes transparent to the laser light, providing a route to optically controlling and optimizing ion acceleration and radiation generation. The scheme involves a self-referencing approach to spectral interferometry, in which coherent transition radiation produced at the foil rear interferes with laser light transmitted through the foil. The relative timing of the onset of transmission with respect to the transition radiation generation is determined from spectral fringe spacing and compared to simultaneous frequency-resolved optical gating measurements. The results are in excellent agreement, and are discussed with reference to particle-in-cell simulations of the interaction physics and an analytical model for the onset time of transparency in ultrathin foils.

I. INTRODUCTION

Ultrabright sources of high energy particles and radiation driven by intense laser pulses are opening up scientific applications (e.g. ultrafast imaging [1–3], high-flux neutron generation [4, 5] and material damage studies [6]), and have wide-ranging potential applications in medicine, security and industry [7, 8]. Much of the research into the development of these sources focuses on interactions in which the target plasma is either wholly transparent (gaseous) or opaque (solid) to the laser pulse over the full interaction. In recent years, there is growing interest in the use of ultrathin foil targets that are initially opaque and dynamically evolve over the course of the interaction to become relativistically transparent to the intense laser light - a process termed relativistic self-induced transparency (RSIT) [9, 10]. This has been shown to result in high ion energies [11, 12], new degrees of control over collective electron dynamics and electrostatic fields in the plasma [13], changes to the spatial distribution of the ion beam [14] and the generation of higher order modes of intense light [15].

Key to optimising radiation generation in ultrathin foils undergoing transparency is control over the point in the interaction at which RSIT occurs [12, 16]. Early in the interaction the plasma density, n_e, is above a critical value, $n_c = m_e\epsilon_0\omega_L^2/e^2$, where $-e$ is the electron charge, m_e is the electron rest mass, ϵ_0 is the vacuum permittivity and ω_L is the angular frequency of the laser light [17]. Bunches of energetic electrons are injected into the foil via mechanisms such as 'Brunel' heating (at ω_L) [18] and $\mathbf{j}\times\mathbf{B}$ heating (at $2\omega_L$) [19, 20]. As the train of bunches exit the target they emit optical radiation in the form of coherent transition radiation (CTR) [21–25]. The production of CTR will start early in the interaction and peak at the maximum of the laser pulse intensity, when the energy transfer to electrons is greatest (there is minimal delay arising from electron transport within an ultrathin foil). At relativistic laser intensities, the mass of the plasma electrons oscillating in response to the intense laser light increases by the Lorentz factor γ_e. As the laser pulse intensity increases in time on the rising edge of the laser pulse, γ_e will increase. Moreover, in the case of ultrathin foils, the thermal pressure causes the plasma to expand, decreasing n_e along the laser axis. γ_e and n_e thus evolve over the course of the interaction between the laser pulse and the plasma, and at the point in time that the condition $n_e < \gamma_e n_c$ is satisfied the plasma becomes relativistically transparent to the laser light, enabling the remainder of the pulse to propagate through it. Precisely when this occurs depends on the degree of plasma heating, and thus laser pulse parameters such as the temporal-intensity profile, polarization and incident angle, and how quickly the plasma expands, which also depends on target properties such as density and thickness. This can occur on the rising or falling edge of the laser pulse interaction with the foil. The fraction of the pulse that is transmitted will further heat the electron population over its propagation length, enhancing the electrostatic fields responsible for ion acceleration [26]. The time at which RSIT occurs with respect to the peak of the laser pulse determines the fraction of the transmitted laser pulse energy and the degree of enhancement in the electrostatic field strength. Controlling the onset time of RSIT is therefore important for optimising ion acceleration in transparency-enhanced acceleration

* paul.mckenna@strath.ac.uk

mechanisms such as Breakout Afterburner (BOA) [27] and hybrid acceleration schemes [12]. It is also important for radiation pressure acceleration [28], for which energy coupling to ions is most efficient at densities just above the threshold for RSIT. In addition, it has recently been shown to be important in tailoring the polarization and spatial mode properties of intense light produced within the plasma [15].

In this study, the onset time of RSIT in ultrathin foils is investigated experimentally using spectral interferometry. It is shown that the superposition of CTR generated while the foil is still opaque with the laser light transmitted through the foil (when RSIT occurs) produces fringes in the spectrum of the detected light and from this the onset time for RSIT can be determined. The approach is verified by frequency-resolved optical gating (FROG) measurements using a GRENOUILLE [29], and compared to particle-in-cell (PIC) simulation results and calculations using an analytical plasma expansion model. This approach offers a simple and effective route to diagnose, and by extension optimize, the time at which the target becomes transparent, with greater temporal resolution than enabled by the GRENOUILLE. It can thereby be applied in the optimisation of laser-driven ion acceleration and the generation of higher order modes of intense light.

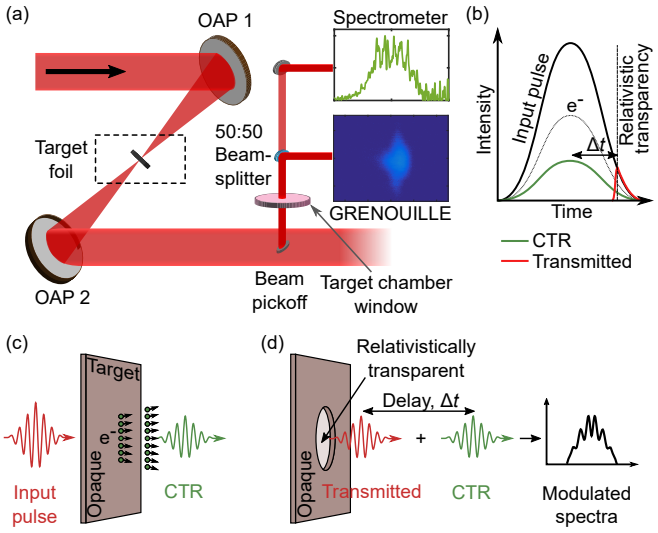

FIG. 1. (a) Schematic of the experiment showing the laser focusing geometry and diagnostic channel. The drive laser pulse is focused using off-axis parabola OAP 1 and the light collected at the target rear, using OAP 2, is directed for simultaneous measurement using a GRENOUILLE and an optical spectrometer. (b) Schematic illustrating the timing of the CTR generation and transmitted part of the laser pulse, where the temporal separation (Δt) relates to the onset time of RSIT relative to the peak of the laser pulse interacting and fast electron generation. (c,d) Schematic of the laser-plasma interaction before, (c), and after, (d), RSIT, resulting in a generated pulse of CTR light and the transmitted laser pulse, with a temporal delay defined by the onset time for RSIT.

II. TEMPORAL PROFILE AND TRANSMISSION MEASUREMENTS

The experiment was performed using the Gemini laser at the Rutherford Appleton Laboratory in the UK. Pulses of linearly-polarized, λ_L=800 nm light (35 nm bandwidth), with energy equal to (3.1±0.2) J (on-target), were focused using a F/2 off-axis parabolic (OAP) mirror to a spot size of (3.9±0.7) μm in diameter (full width at half maximum, FWHM). The calculated peak intensity is $(2.8\pm0.4)\times10^{20}$ Wcm^{-2}. A double plasma mirror enhanced the intensity contrast to $\sim10^{11}$ and $\sim10^{8}$, at 1 ns and 2 ps, respectively, prior to the peak of the pulse. The pulse duration was varied from 40 to 120 fs (FWHM) using an acousto-optic device that adds group delay to the pulse. Example measurements of the laser pulse temporal-intensity profile are provided in the Supplemental Material file [30].

The targets were aluminium foils, with thickness, d, varied in the range 10-100 nm. The overall uncertainty in the foil thickness arises from two sources: a calibrated uncertainty of ±10% in the manufacturing processes (variation in coating a substrate from which the ultrathin foil is released) and ±3 nm due to the accuracy of the step-profilometer measurements of the coating thickness. The targets were irradiated at near-normal incidence.

Light at the rear of the plasma (transmitted and generated) was collected using a F/2, 200 mm diameter OAP (an identical OAP to the one used to focus the laser light onto the target). The set-up is shown in Fig. 1(a). A '0.5-inch' (12.7 mm diameter) high-damage-threshold aluminium mirror (optimized reflectively for 450 nm-20 μm light) was positioned 60 mm from the centre of the beam (sampling ~0.7% of the beam) in the plane of the polarization (i.e. parallel to the polarization axis), and directed the light out of the vacuum chamber through a 1 mm-thick fused silica window (optical quality, with an anti-reflection coating, allowing 99.5% transmission). The size of the pick-off optic was only limited by the use of other diagnostics on the same beam path and, if needed, a larger area of the beam could be sampled. A non-polarizing beam-splitter was used to divide the light into equal fractions for measurements using an optical spectrometer (Avantes) and a GRENOUILLE (Swamp Optics). The percentage of the light signal that is incident on both diagnostics has been calculated as a function of wavelength (in the range 700-900 nm) using the transmission and reflectivity values for each optic in both beam paths, and is available in the Supplemental Material file [30]. CTR components perpendicular to the laser polarization axis were not filtered out in the optical spectrometer beam path. The GRENOUILLE will filter out these components due to the doubling crystal used in the system. A calculation of the non-linear phase shift (B-integral) along the beam path confirms that non-linear propagation effects were negligible for the transmitted

pulse intensities. The temporal direction measured with the GRENOUILLE was established by applying a known frequency chirp (with a known chirp direction) to the pulse.

Figure 1(b) illustrates the temporal sequence for CTR generation and transmitted light (arising from RSIT) relative to the laser pulse profile and Figs. 1(c) and (d) show schematics of the interaction at the stage of CTR generation and laser light transmission during RSIT, respectively. Both light components co-propagate as pulses with a peak-to-peak separation equal to Δt. The divergence of the two components will differ. For the laser intensity range explored in this experiment, and following the model presented in Ref. [23], the divergence of the CTR beam is calculated to be in the range 5-15° (half-angle) and thus smaller than the divergence of the transmitted beam. Both are collected by the OAP, but the final beam divergence will differ. For general application of this approach, the light levels can be changed by suitable choice of optics and beam path. Provided the ratio of the detected CTR and transmitted laser signals is sufficiently close to 1 then clear fringes with good contrast are observed. As shown in the Supplemental Material file [30], even for a ratio as low as 0.2 it is possible to still resolve the frequency of the fringes and therefore make a delay measurement. The technique will not work for cases in which RSIT occurs too early in the interaction, such that there is limited energy coupling to fast electrons, reducing the reference CTR signal, and resulting in a ratio of less than ∼0.2.

Figure 2 shows representative GRENOUILLE measurements for three cases (a) no target, i.e. the reference incident laser pulse, (b) d =37 nm, and (c) d =30 nm. The signal for the d =37 nm target is dominated by the CTR emission (negligible transmission measured). As the target thickness is decreased to 30 nm, RSIT starts to occur, late in the interaction, resulting in the transmission of a small fraction of the laser light, with intensity comparable to the CTR. The total measured light signal (transmitted plus CTR) is plotted as a function of target thickness in Fig. 3(a) [15]. d=30 nm represents a threshold thickness at which RSIT starts to occur and the measured intensity of the light is observed to rapidly increase with decreasing target thickness below this value. The autocorrelation image measurement in Fig. 2(c) shows a triple-pulse structure, which is equivalent to a double-pulse in time when processed by the GRENOUILLE pulse-retrieval algorithm [29]. The fringes in the spectral direction of the raw GRENOUILLE image (Fig. 2(c)) is another signature of the presence of multiple pulses.

Measurements were made for input pulse durations of τ_L =40 fs, 80 fs and 120 fs, for d=30 nm. At this thickness, the measured degree of transmission increases with pulse duration, as shown in Fig. 3(b). Despite the decrease in the peak laser intensity, with increasing pulse duration the target expands more over the interaction, enabling RSIT to occur earlier. In Fig. 2(d), the corresponding temporal profiles measured using the

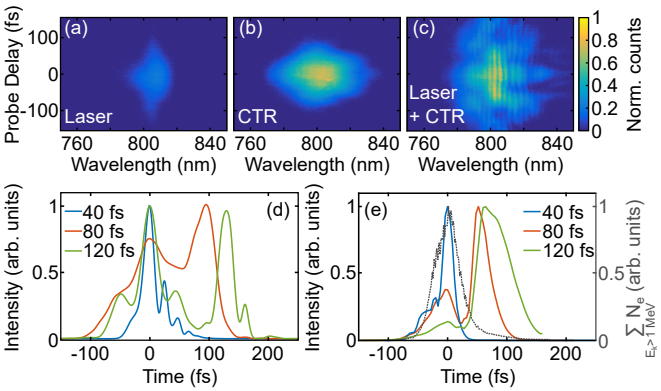

FIG. 2. FROG measurements of the transmitted and/or generated light for: (a) no target; (b) d =37 nm; (c) d =30 nm; all for τ_L=40 fs. (d) Temporal-intensity profile of light measured at the target rear side extracted from example GRENOUILLE measurements for d =30 nm, for three given durations of the drive laser pulse. (e) Corresponding results from 3D EPOCH PIC simulations, including a plot of the total number of electrons (with energy >1 MeV) as a function of time, for the 80 fs pulse duration case.

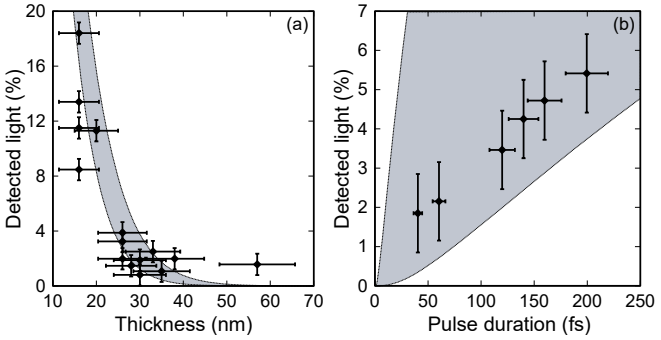

FIG. 3. Measured light level at the target rear as a percentage of the incident laser pulse energy as a function of (a) target thickness, for τ_L=40 fs, and (b) pulse duration, for d =30 nm. The grey band corresponds to calculations of the upper and lower bounds using the model reported in Yan *et al.* [31], with the limits defined by the uncertainty in intensity in the experiment in (a) and the uncertainties in intensity and target thickness in (b).

GRENOUILLE are shown. For τ_L =40 fs, the reconstructed pulse is dominated by a single pulse centred at t =0 fs. For τ_L =80 fs the appearance of a second pulse, peaked at 80 fs, is apparent. For τ_L =120 fs, the second pulse is still present, but delayed to t ∼120 fs. Reference measurements were made of the input pulse profile without a target in place for each τ_L and for all cases a single pulse is measured. It is clear from these measurements that the onset of RSIT in an ultrathin foil results in two pulses of light co-propagating along the laser axis.

In Fig. 3, calculations of the expected degree of light transmission, made using the plasma expansion model introduced by Yan *et al.* [31] to describe transparency and ion acceleration in ultrathin foils, are in-

cluded alongside the measurements as the shaded region. In that model, the onset time for RSIT is given as $t_{RSIT} = (12/\pi^2)^{1/4}(n_e\tau_L d/(n_c a_0 C_s))^{1/2}$, where a_0 is the normalized laser amplitude, $C_s = \sqrt{Zm_e c^2 a_0/m_i}$ is the ion sound speed and Z is the ion charge state. The upper and lower bounds of the shaded regions in Fig. 3 are defined by the experimental uncertainties in laser intensity and target thickness. The measured scaling with target thickness and pulse duration are in broad agreement with the model calculations, noting that the measurements include the CTR light, whereas the model is for transmitted light only.

III. SIMULATIONS OF TWO-PULSE GENERATION

We performed 3D PIC simulations using the EPOCH code [32] to investigate the source of the pulses. The grid comprised of 1000 × 720 × 720 mesh cells, corresponding to 20 μm × 20 μm × 20 μm. The laser pulse parameters were chosen to closely approximate the experiment; λ_L=800 nm; linear polarization; Gaussian temporal profile with τ_L varied in the range 40-120 fs (FWHM); 3 μm focal spot. The peak intensity was 2×10^{20}-6×10^{20} Wcm^{-2} (varied corresponding to the changes in pulse duration), such that the light level transmitted through the target approximately matched the experimental results. Time t=0 fs corresponds to the peak of the laser pulse interacting with the center of the target.

The target comprised of a 30 nm-thick layer of Al^{13+} ions with a 6 nm-thick layer of mixed C^{6+} and H^+ ions on the surfaces to mimic the presence of hydrocarbon contaminants in the experiment. To approximate the effect of the laser temporal-intensity contrast, the electron and ion populations were pre-expanded to a Gaussian profile such that for a given target thickness d, the maximum electron density was $30n_c$ (the areal density was kept equivalent to initially solid density aluminium, $444n_c$, at the given target thickness). Further simulation details are provided in the Supplementary Material file [30].

The simulations reveal that the first pulse of light at the target rear is CTR produced by relativistic electrons crossing the target-vacuum boundary and that the second (later) peak is the portion of the laser pulse transmitted due to RSIT. This is verified for thick targets for which transparency does not occur and only the first pulse is observed. The CTR signal increases with increasing laser intensity on the pulse rising edge and is found to peak very close to t=0 fs, the peak of the laser pulse interaction. The conversion of laser energy to bunched electrons is highest at this time and, as the target is ultrathin, there is no delay in CTR generation due to electron transport. Thus, the temporal delay measured is the temporal separation between the peak of the incident laser pulse intensity profile, at which conversion to fast electrons and thus CTR emission is maximised, and the peak of the transmitted portion of the laser light. Note that if transparency were to occur on the rising edge of the laser pulse interaction, the CTR signal would still be increasing when the remainder of the laser light is transmitted, and thus spectral interference would not be observed. This diagnostic approach works when transparency occurs after the peak of the interaction. The delay in transparency with respect to the peak of the laser pulse interaction is a key figure of merit for the optimisation of electron and ion acceleration in the RSIT regime [12].

The temporal pulse profile extracted from the simulations is shown in Fig. 2(e). A spatial Fourier transform was taken of the grid and filtered for the laser wavelength. A longitudinal sample window 6 μm wide, centred at 3 μm from the target surface, was then taken and the squared transverse electric field components integrated. This was calculated for every 4 fs time step. Although the simulation parameters are idealised, the results demonstrate a similar behaviour to the measured pulse profiles in Fig. 2(d). Only the CTR pulse is observed for the shortest pulse duration case, τ_L =40 fs. The transmitted laser pulse becomes apparent as the pulse duration is increased, because the time over which the target becomes transparent also increases. The temporal evolution of the total number of fast electrons above 1 MeV is shown for the τ_L=80 fs case and can be seen to correlate with the first pulse, demonstrating that this pulse is due to CTR emission. For the τ_L=120 fs case, Δt is measured to be ∼120 fs in the experiment and ∼100 fs in the simulations. The small difference is due to the predefined expansion in the simulation not precisely matching that of the experiment, which is driven by the rising edge profile of the laser pulse.

IV. SPECTRAL INTERFERENCE MEASUREMENTS

Having established the source of the two pulses and the close correlation of Δt to the time at which RSIT occurs, we now investigate the case in which RSIT occurs relatively late in the interaction. In Fig. 4(a), the temporal profile measured with the GRENOUILLE is shown for the interaction of an τ_L=∼40 fs pulse with targets with d =28-37 nm. This is a small thickness range, but is sufficient to observe the transition from targets which remain opaque over most of the interaction to those that exhibit some transparency. While the d =37 nm target appears to be opaque (i.e there is no second pulse measured) both the d =28 nm and d =35 nm targets undergo RSIT, with Δt=∼40 fs and ∼50 fs, respectively. Importantly, these measurements demonstrate that near the threshold conditions for the onset of RSIT the two pulses are only just resolvable by the GRENOUILLE, unlike the case in Fig. 2(d). This is due to the temporal resolution of the GRENOUILLE and its limited dynamic range.

By introducing a separate spectrometer into the diagnostic beam path, as illustrated in Fig. 1(a), detailed

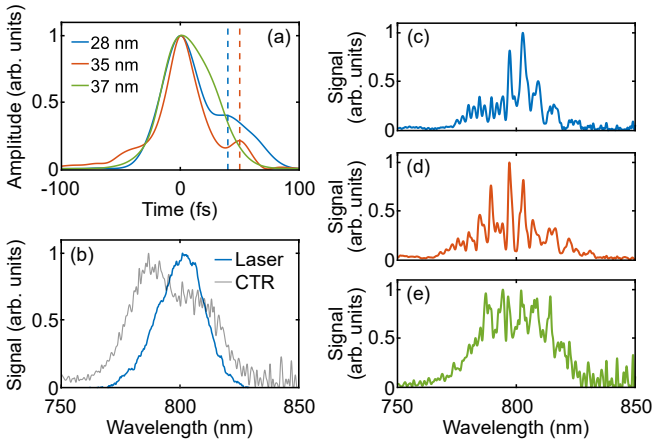

FIG. 4. (a) Temporal-intensity profile extracted from GRENOUILLE measurements for three given target thicknesses, for fixed drive laser pulse duration τ_L=40 fs. (b) Representative measurements of the input laser spectrum and the generated CTR spectrum. (c-e) Spectral measurements for: (c) d =28 nm; (d) d =35 nm; and (e) d =37 nm targets.

measurements of the transmitted pulses can be made in the frequency domain with greater sensitivity and resolution than is possible with the GRENOUILLE. For reference, the measured spectra for a single laser pulse and a single CTR pulse (on separate shots) is shown in Fig. 4(b). In Fig. 4(c-e) the measured spectra for the d =25 nm, d =35 nm and d =37 nm targets are shown. These spectra all contain fringes that are not present in the reference spectra. These fringes are a clear signature of the interference of two pulses [33]. Spectral fringes are also observed for the 37 nm target, but with smaller amplitude, suggesting the presence of a second, weak pulse that is not detected using the GRENOUILLE. Note that for practical considerations (due to the differing levels of sensitivity of the two diagnostics to the very small amount of laser light transmitted in this target thickness range), the data shown in Fig. 4(c-e) are for different laser shots to that shown in Fig. 2. The optical spectrometer measurements corresponding to the data in Fig. 2 are available in the Supplemental Material file [30].

V. DIAGNOSING TRANSPARENCY

Spectral interferometry is a well established technique. It is used for example in the SPIDER [34] pulse reconstruction methodology, in the TADPOLE technique [35] and has previously been used to accurately temporally overlap two short pulses [36]. Of particular relevance here is its use in the research reported in Bagnoud *et al.* [37] to investigate laser-foil interactions in the RSIT regime. That work differs from the present in that a double laser pulse (500 fs duration pulses separated by 3 ps) was used and the resulting spectral interference was measured when both pulses are transmitted through the foil. By using the interference of the self-generated CTR light and the transmitted laser pulse, our approach enables investigation of the onset of RSIT close to threshold conditions and without changing the drive laser pulse parameters.

The fringes in the spectrum result from interference between the two pulses. It is straightforward to show that the summation of two pulses, $E_{CTR}(t) = E_{0(CTR)}e^{-i(\omega\tau+\phi_{CTR})}$ and $E_L(t) = E_{0(L)}e^{-i(\omega\tau+\phi_L)}$, in the frequency domain is:

$$S_{CTR+L}(\omega) = |\mathcal{F}(E_{CTR}(t) + E_L(t))|^2 = E_{0(CTR)}(\omega)^2 + E_{0(L)}(\omega)^2 + 2E_{0(CTR)}(\omega)E_{0(L)}(\omega)\cos(\omega\Delta t + \Delta\phi) \quad (1)$$

where, in the simplest case, $E_{0(CTR)}(t) = E_{0(L)}(t) = e^{(-(t-t_0)/2\sigma^2)}$, $\sigma = \tau_L/2\sqrt{\ln(2)}$ and τ_L is the duration (FWHM) of the respective pulses. The oscillatory $\cos(\omega\Delta t + \Delta\phi)$ term produces fringes in the spectrum. Note that in the present case, CTR is maximised at the peak of the drive laser pulse interaction and thus Δt corresponds to the time delay until RSIT occurs and the remainder of the laser light is transmitted through the plasma. As the simulations show that the transmitted portion of the pulse has a very fast rising edge, Δt effectively corresponds to the time at which RSIT occurs relative to the peak of the laser pulse interaction.

Using this approach, a model was developed to investigate the expected spectral features for the superposition of two pulses. For simplicity, we consider two identical transform-limited Gaussian pulses with equal amplitude, zero phase difference and τ_L=40 fs. In this model we assume that regardless of the onset of transparency, the incident laser always gives rise to a CTR reference signal of similar duration, peaking at the maximum of the laser pulse intensity profile. For the sake of simple analysis, the transmitted laser pulse is assumed to have a predominantly Gaussian shape and any self-phase modulation of the pulse arising from propagation in the plasma or in the diagnostic line is small and considered a second order effect. Deviations are assumed to only lead to small increases in systematic errors. Due to the very thin targets used, any additional delay induced between the two pulses due to the time difference between the production of CTR and the propagation of the laser through the target is assumed to be negligible. Similarly, any delays caused by propagation through the expanding underdense preplasma are assumed to be negligible. Finally, any self-phase modulation is neglected in the model. Note that we have established that self-phase modulation does not play a role in the experimental results reported.

An example spectra obtained using this model is shown in Fig. 5(a) for Δt=150 fs. By scanning Δt it is possible to observe the change in the periodicity of the spectral fringes. This is shown in Fig. 5(b) as a Δt-wavelength plot, with the spectral intensity shown by the coloured axis. The inverse Fourier transform of the calculated

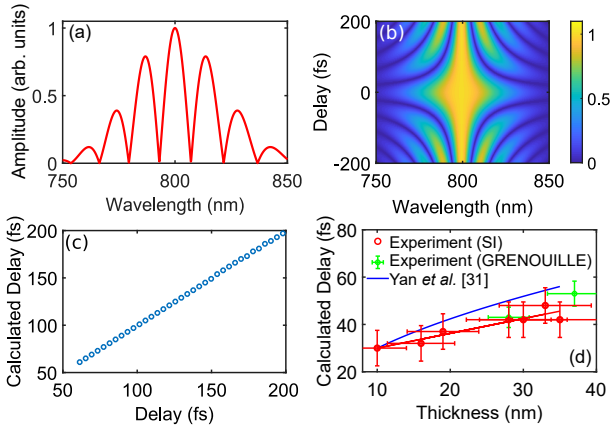

FIG. 5. (a) Model spectrum for the superposition of two identical pulses with τ_L =40 fs and Δt=150 fs, illustrating spectral fringes. (b) Spectral fringe pattern as a function of Δt, from -200 to 200 fs. (c) Calculated delay from a Fourier transform of the spectrum, as a function of the input delay. (d) Delay determined from a Fourier transform of the measured spectra in the experiment, as a function of target thickness (red points) and the points measured using the GRENOUILLE (for comparison), for τ_L=40 fs. Calculated time for the target to become transparent to the laser using the plasma expansion model reported in Yan *et al.* [31] (blue).

spectrum enables the delay (separation) between the two pulses to be determined, to test the approach. Excellent agreement is obtained between the input delay and the delay calculated using this method, as shown in Fig. 5(c).

We next extracted the values of Δt from the spectral interference data shown in Fig. 4(c-e) and for additional thicknesses not shown. The results of this analysis are shown in Fig. 5(d). The error bars shown in the target thickness are defined by the degree of uncertainty in the characterization of the ultrathin foils. The uncertainty in the calculated delay is determined from the spectral resolution of the spectrometer and CCD (0.5 nm/pixel). We calculate the change in the delay needed to modify the fringe spacing by 0.5 nm to be $\pm$7.5 fs. Note that use of a higher resolution optical spectrometer or CCD detector would improve the temporal resolution. Δt is observed to increase with target thickness, from Δt=32 fs for d =16 nm to Δt=48 fs for d =33 nm. These values are consistent with those measured using the GRENOUILLE, shown in Fig. 5(d) (in green), and those obtained from the PIC simulations (e.g. Δt=48 fs for d =33 nm).

We include the calculated onset time for RSIT from the plasma expansion model introduced by Yan *et al.* [31] (discussed above), in Fig. 5(d). We find that, despite the 1D nature of the model, the predictions are in good overall agreement with our measurements, particularly for the thinnest targets investigated.

VI. SUMMARY

In summary, we report on experimental measurements of the time at which expanding ultrathin foils become relativistically transparent to intense laser light, as diagnosed using a self-referencing approach to spectral interferometry. With reference to GRENOUILLE measurements, we show how the generation of CTR light, which is maximised at the peak of the laser pulse interaction, provides a reference signal against which the temporal delay in the onset of RSIT can be measured. We find good agreement with 3D PIC simulations of the interaction, verifying the approach, and compare our results with an analytical model of plasma expansion dynamics.

This approach in principle enables the onset time of relativistic transparency to be determined to within a few femtoseconds and, because it is self-referencing, without modification of the drive laser pulse. Furthermore, it is easy to set up and operate (requiring only a collection optic, beam steering optics and an optical spectrometer) and, because the data collection and analysis can be automated, there is potential to include it in experiments applying active feedback [38, 39]. It will enable tuning of the laser and target parameters to control the onset of transparency and thus the optimization of promising ion acceleration mechanisms involving ultrathin foils, and the manipulation of the polarization and spatial mode structure of intense light produced within the plasma.

ACKNOWLEDGMENTS

We acknowledge the expertise of the staff at the Central Laser Facility, Rutherford Appleton Laboratory. The research was supported by EPSRC (EP/R006202/1 and EP/M018091/1) and used the ARCHER and ARCHIE-WeSt high performance computers, with access provided via the Plasma Physics HEC Consortia (EP/R029148/1). EPOCH was developed under EPSRC grant EP/G054940/1. Data associated with research published in this paper can be accessed at https://doi.org/10.15129/2052ff71-2c9b-447a-a1f1-b97e319186d3.

[1] L. Romagnani, J. Fuchs, M. Borghesi, P. Antici, P. Audebert, F. Ceccherini, T. Cowan, T. Grismayer, S. Kar, A. Macchi *et al.*, Dynamics of Electric Fields Driving the Laser Acceleration of Multi-MeV Protons, Phys. Rev. Lett. 95, 4 (2005).

[2] S. Kneip, C. McGuffey, F. Dollar, M. S. Bloom, V. Chvykov, G. Kalintchenko, K. Krushelnick, A. Maksimchuk, S. P. D. Mangles, T. Matsuoka *et al.*, X-ray phase contrast imaging of biological specimens with femtosecond pulses of betatron radiation from a compact laser plasma wakefield accelerator, Appl. Phys. Lett. 99, 093701 (2011).

[3] J. C. Wood, D. J. Chapman, K. Poder, N. C. Lopes, M. E. Rutherford, T. G. White, F. Albert, K. T. Behm, N. Booth, J. S. J. Bryant *et al.*, Ultrafast Imaging of Laser Driven Shock Waves using Betatron X-rays from a Laser Wakefield Accelerator, Sci. Reports 8, 11010 (2018).

[4] M. Roth, D. Jung, K. Falk, N. Guler, O. Deppert, M. Devlin, A. Favalli, J. Fernandez, D. Gautier, M. Geissel *et al.*, Bright Laser-Driven Neutron Source Based on the Relativistic Transparency of Solids, Phys. Rev. Lett. 110, 1 (2013).

[5] S. Kar, A. Green, H. Ahmed, A. Alejo, A. P. L. Robinson, M. Cerchez, R. Clarke, D. Doria, S. Dorkings, J. Fernandez *et al.*, Beamed neutron emission driven by laser accelerated light ions, New J. Phys., 18, 053002 (2016).

[6] B. Dromey, M. Coughlan, L. Senje, M. Taylor, S. Kuschel, B. Villagomez-Bernabe, R. Stefanuik, G. Nersisyan, L. Stella, J. Kohanoff *et al.*, Picosecond metrology of laser-driven proton bursts, Nat. Comms. 7, 3 (2016).

[7] P. Bolton, K. Parodi and J. Schreiber *Applications of laser-driven particle acceleration* (CRC Press, Taylor and Francis, 2018).

[8] C. M. Brenner, S. R. Mirfayzi, D. R. Rusby, C. Armstrong, A. Alejo, L. A. Wilson, R. Clarke, H. Ahmed, N. M. H. Butler, D. Haddock *et al.*, Laser-driven x-ray and neutron source development for industrial applications of plasma accelerators, Plasma Phys. Control. Fusion 58, 014039 (2016).

[9] V. A. Vshivkov, N. M. Naumova, F. Pegoraro and S. V. Bulanov, Nonlinear electrodynamics of the interaction of ultra-intense laser pulses with a thin foil, Phys. Plasmas 5, 2727 (1998).

[10] V. I. Eremin, A. V. Korzhimanov and A. V. Kim, Relativistic self-induced transparency effect during ultraintense laser interaction with overdense plasmas: Why it occurs and its use for ultrashort electron bunch generation, Phys. Plasmas 17, 043102 (2010).

[11] J. C. Fernández, D. C. Gautier, C. Huang, S. Palaniyappan, B. J. Albright, W. Bang, G. Dyer, A. Favalli, J. F. Hunter, J. Mendez *et al.*, Laser-plasmas in the relativistic-transparency regime: Science and applications, Phys. Plasmas 24, (2017).

[12] A. Higginson, R. J. Gray, M. King, R. J. Dance, S. D. R. Williamson, N. M. H. Butler, R. Wilson, R. Capdessus, C. Armstrong, J. S. Green *et al.*, Near-100 MeV protons via a laser-driven transparency-enhanced hybrid acceleration scheme, Nat. Commun. 9, (2018).

[13] B. Gonzalez-Izquierdo, R. J. Gray, M. King, R. J. Dance, R. Wilson, J. McCreadie, N. M. H. Butler, R. Capdessus, S. Hawkes, J. S. Green, *et al.*, Optically controlled dense current structures driven by relativistic plasma aperture-induced diffraction, Nat. Phys. 12, (2016).

[14] B. Gonzalez-Izquierdo, M. King, R. J. Gray, R. Wilson, R. J. Dance, H. Powell, D. A. MacLellan, J. McCreadie, N. M. H. Butler, S. Hawkes *et al.*, Towards optical polarization control of laser-driven proton acceleration in foils undergoing relativistic transparency, Nat. Commun. 7, 1 (2016).

[15] M. J. Duff, R. Wilson, M. King, B. Gonzalez-Izquierdo, A. Higginson, S. D. R. Williamson, Z. E. Davidson, R. Capdessus, N. Booth, S. Hawkes *et al.*, High order mode structure of intense light fields generated via a laser-driven relativistic plasma aperture, Sci. Reports, 10, 105 (2020).

[16] S. Palaniyappan, B. M. Hegelich, H.-C. Wu, D. Jung, D. C. Gautier, L. Yin, B. J. Albright, R. P. Johnson, T. Shimada, S. Letzring*et al.*, Dynamics of relativistic transparency and optical shuttering in expanding overdense plasmas, Nat. Phys. 8, 763 (2012).

[17] F. Chen, in *Introduction to Plasma Physics and Controlled Fusion* (Plenum Publishing Corporation, 1984), Vol. 1, 2nd ed.

[18] F. Brunel, Not-so-resonant, resonant absorption, Phys. Rev. Lett. 59, 52 (1987).

[19] S. D. Baton, J. J. Santos, F. Amiranoff, H. Popescu, L. Gremillet, M. Koenig, E. Martinolli, O. Guilbaud, C. Rousseaux, M. Rabec Le Gloahec *et al.*, Evidence of Ultrashort Electron Bunches in Laser-Plasma Interactions at Relativistic Intensities, Phys. Rev. Lett. 91, 1 (2003).

[20] H. Popescu, S. D. Baton, F. Amiranoff, C. Rousseaux, M. Rabec Le Gloahec, J. J. Santos, L. Gremillet, M. Koenig, E. Martinolli, T. Hall *et al.*, Subfemtosecond, coherent, relativistic, and ballistic electron bunches generated at ω_0 and $2\omega_0$ in high intensity laser-matter interaction, Phys. Plasmas 12, 1 (2005).

[21] J. J. Santos, F. Amiranoff, S. D. Baton, L. Gremillet, M. Koenig, E. Martinolli, M. Rabec Le Gloahec, C. Rousseaux, D. Batani, A. Bernardinello *et al.*, Fast Electron Transport in Ultraintense Laser Pulse Interaction with Solid Targets by Rear-Side Self-Radiation Diagnostics, Phys. Rev. Lett. 89, 025001 (2002).

[22] C. Bellei, S. R. Nagel, S. Kar, A. Henig, S. Kneip, C. Palmer, A. Sävert, L. Willingale, D. C. Carroll, B. Dromey *et al.*, Micron-scale fast electron filaments and recirculation determined from rear-side optical emission in high-intensity laser-solid interactions, New J. Phys. 12, (2010).

[23] C. Bellei, J. R. Davies, P. K. Chauhan and Z. Najmudin, Coherent transition radiation in relativistic laser–solid interactions, Plasma. Phys. Control. Fusion 54, 035011 (2012).

[24] C. B. Schroeder, E. Esarey, J. van Tilborg and W. P. Leemans, Theory of coherent transition radiation generated at a plasma-vacuum interface, Phys. Rev. E 59, 016501 (2004).

[25] J. Zheng, K. A. Tanaka, T. Sato. T. Yabbuchi, T. Kurahashi, Y. Kitawaga, R. Kodama, T. Norimatsu and T. Yamanaka, Study of Hot Electrons by Measurement of Optical Emission from the Rear Surface of a Metallic Foil Irradiated with Ultraintense Laser Pulse, Phys. Rev. Lett. 92, 165001 (2004).

[26] S. D. R Williamson, R. J. Gray, M. King, R. Wilson, R. J. Dance, C. Armstrong, D. R. Rusby, C. Brabetz, F. Wagner, B. Zielbauer *et al.*, Energy absorption and coupling to electrons in the transition from surface- to volume-dominant intense laser-plasma interaction regimes. New J. Phys. 22, 053044 (2020).

[27] L. Yin, B. J. Albright, B. M. Hegelich and J. C. Fernandez, GeV laser ion acceleration from ultrathin targets: The laser break-out afterburner, Laser Part. Beams 24, 291 (2006).

[28] S. S. Bulanov, E. Esarey, C. B. Schroeder, S. V. Bulanov, T. Zh. Esirkepov, M. Kando, F. Pegoraro and W. P. Leemans, Radiation pressure acceleration: The factors limiting maximum attainable ion energy, Phys. Plasmas 23, 056703 (2016).

[29] R. Trebino, in *Frequency-Resolved Optical Gating: The Measurement of Ultrashort Laser Pulses* (Kluwer Academic Publishers, Boston, 2002).

[30] See Supplemental Material at [URL will be inserted by publisher] for further details on experiment and numerical methodology.

[31] X. Q. Yan, T. Tajima, M. Hegelich, L. Yin and D. Habs, Appl. Theory of laser ion acceleration from a foil target of nanometer thickness, Phys. B Lasers Opt. 98, 711 (2010).

[32] T. D. Arber, K. Bennett, C. S. Brady, A. Lawrence-Douglas, M. G. Ramsay, N. J. Sircombe, P. Gillies, R. G. Evans, H. Schmitz, A. R. Bell *et al.*, Contemporary particle-in-cell approach to laser-plasma modelling, Plasma Phys. Control. Fusion 57, 113001 (2015).

[33] C. Froehly, A. Lacourt and J. C. Vienot, Time impulse response and time frequency response of optical pupils.:Experimental confirmations and applications, Nouvelle Revue d'Optique, 4(4), 183. (1973).

[34] C. Iaconis and I. A. Walmsley, Spectral phase interferometry for direct electric-field reconstruction of ultrashort optical pulses, Opt. Lett. 23, 792-794 (1998).

[35] D. N. Fittinghoff, J. L. Bowie, J. N. Sweetser, R. T. Jennings, M. A. Krumbügel, K. W. DeLong, R. Trebino and I. A. Walmsley, Measurement of the intensity and phase of ultraweak, ultrashort laser pulses, Opt. Lett. 21, 1313 (1996).

[36] D. J. Corvan, T. Dzelzainis, C. Hyland, G. Nersisyan, M. Yeung, M. Zepf and G. Sarri, Optical measurement of the temporal delay between two ultra-short and focussed laser pluses, Opt. Express 24, 3127-3136 (2016).

[37] V. Bagnoud, J. Hornung, T. Schlegel, B. Zielbauer, C. Brabetz, M. Roth, P. Hilz, M. Haug, J. Schreiber and F. Wagner, Studying the Dynamics of Relativistic Laser-Plasma Interaction on Thin Foils by Means of Fourier-Transform Spectral Interferometry, Phys. Rev. Lett. 118, 255003 (2017).

[38] S. J. D. Dann, C. D. Baird, N. Bourgeois, O. Chekhlov, S. Eardley, C. D. Gregory, J.-N. Gruse, J. Hah, D. Hazra, S. J. Hawkes *et al.*, Laser wakefield acceleration with active feedback at 5 Hz, Phys. Rev. Acc. Beams 22, 041303 (2019).

[39] A. Schienker, S. Gessner, C. Emma and A. L. Edelen, Adaptive model tuning studies for non-invasive diagnostics and feedback control of plasma wakefield acceleration at FACET-II, Nucl. Instrum. Methods Phys. Res. A. 967, 163902 (2020)